Applied Catalysis B: Environmental 89 (2009) 557–562

Contents lists available at ScienceDirect

Applied Catalysis B: Environmental

journal homepage: www.elsevier.com/locate/apcatb

Photo-induced charging effect and electron transfer to the redox species on nitrogen-doped TiO_2 under visible light irradiation

Shinya Higashimoto *, Masashi Azuma

Department of Applied Chemistry, College of Engineering, Osaka Institute of Technology, 5-16-1 Omiya, Asahi-ku, Osaka 535-8585, Japan

ARTICLE INFO

Article history:
Received 1 November 2008
Received in revised form 16 January 2009
Accepted 22 January 2009
Available online 2 February 2009

Keywords:
Nitrogen-doped TiO_2
Photocatalyst
Visible light
Photo-charging
Photo-electrochemistry
Charge separation
Redox potential
Electron transfer

ABSTRACT

Energy levels for sub-band structures of the nitrogen-doped TiO_2 (N-TiO_2) and photo-excitation mechanism for the visible light response were investigated by photo-electrochemical and spectroscopic measurements. It was demonstrated that the photo-excitation from the N-doping level of N-TiO_2 causes the accumulation of electrons into the sub-band level at the potential energy of ca. +0.35 V vs. NHE (pH 2.5) under visible light irradiation. Subsequently, electron transfer does not take place from the photo-charged N-TiO_2 under visible light irradiation into such redox species as methyl viologen (MV^{2+}), H^+, Cu^{2+} ions, but into O_2 molecules, Pt^{4+}, Ag^+ and Au^{3+} ions by way of the sub-band level. These findings shed light on a mechanism for the photocatalytic reactions on the N-TiO_2 under visible light irradiation.

© 2009 Elsevier B.V. All rights reserved.

1. Introduction

Titanium dioxide (TiO_2) is the most extensively investigated material in the field of photocatalysis. Since the band gap of TiO_2 having anatase structure is ca. 3.2 eV, it can be only activated by UV–vis irradiation, which is given ca. 4% on the earth's surface from the sun. Therefore, several attempts have been made to realize photo-functional materials that work under visible light irradiation in order to improve the utilization of solar energy [1–5]. One of the most promising visible-light responsive photocatalyst is nitrogen-doped TiO_2 (N-TiO_2). It has been synthesized by such methods as sol–gel and heat treatment of TiO_2 in a flow of NH_3, and has been characterized by such techniques as XPS, ESR, FT-IR, photo-electrochemical measurement and theoretical calculation [5–31].

For the mechanism of visible light response, Livraghi et al. investigated the origin of photo-activity of N-TiO_2 by a combined experimental and theoretical approach [20]. It was proposed that nitrogen species involved in N-TiO_2 is responsible for visible light absorption with promotion of electrons from the band gap localized states to the conduction band or to surface adsorbed electron scavengers. On the other hand, the photo-electrochemical measurements by Sakthivel et al. showed not only the band gap narrowing of 40–80 meV, but also the anodic shift of quasi Fermi potential of 40–90 mV [13]. Furthermore, Nakamura et al. showed the mechanism for the visible light response in the anodic photocurrent by the photo-electrochemical measurements, and suggested that the photo-excitation from the nitrogen doping level located at ca. +0.75 eV above valence band to the conduction band [12].

For the photocatalytic performance of N-TiO_2, amounts of nitrogen species doped in N-TiO_2 is important factor to improve photocatalytic activity, and excess nitrogen species causes the decrease of the activity [9]. These results indicate that the more creation of oxygen vacancies (OVs) by doping nitrogen owing to charge compensation causes the more charge recombination or electron trapping. In order to suppress the charge recombination or electron trapping, it was previously reported that the N-TiO_2 surface modification by redox mediators as platinum, vanadium, iron and copper species enhances the photocatalytic activities under visible light irradiation compared with N-TiO_2 by itself [24–26]. So far, few studies on reductive potentials of the photo-excited N-TiO_2 have been systematically investigated, although the studies on oxidative potentials were investigated by Nakamura et al. [12]. Along these lines, it is important to understand, in particular, from what energy levels the photo-induced electrons on N-TiO_2 work for the reduction of redox species under visible light irradiation.

Here, we report on the energy levels for sub-band structures of N-TiO_2, and on the photo-excitation mechanism by the combination

* Corresponding author.
E-mail address: higashimoto@chem.oit.ac.jp (S. Higashimoto).

0926-3373/$ – see front matter © 2009 Elsevier B.V. All rights reserved.
doi:10.1016/j.apcatb.2009.01.017

of photo-electrochemical and spectroscopic measurements. It is paid attention to electron transfer from the photo-induced N-TiO_2 surface under visible light irradiation into various redox species.

2. Experimental

2.1. Sample preparation

The N-TiO_2 materials were facilely prepared by the hydrolysis of tetra-isopropyl titanate (TTIP) with an ammonium aqueous solution (28–30 wt% as NH_3). Pure TiO_2 materials were prepared by the hydrolysis of TTIP with water. Both products were washed several times with distilled water, recovered by filtration, and dried at 343 K for 12 h, followed by calcination at 673 K for 3 h in air.

2.2. Sample characterizations

The powder X-ray diffraction (XRD) patterns were obtained with a RIGAKU RINT2000 using Cu Kα radiation (λ = 1.5417 Å). The crystallite size of TiO_2 was estimated by the Scherer equation. The X-ray photoelectron spectroscopic (XPS) measurements were performed with a KRATOS, AXIS Ultra spectrometer using Al Kα radiation (E = 1486.8 eV). The UV–vis spectroscopic measurements were carried out on the diffuse reflectance mode with a UV–vis scanning spectrophotometer, UV-3100PC, Shimadzu. The collected data were converted into absorbance vs. photoenergy (eV). The photoluminescence measurements were carried out by a Spex Fluorolog-3 spectrofluorometer with a light source (xenon lamp). A band-path for excitation and emission was adjusted at 5.0 nm, respectively. Prior to measurements, a sample was evacuated at room temperature up to $<10^{-1}$ Pa in the quartz tube. Excitation and emission spectra of the sample were taken at liquid nitrogen temperature.

2.3. Electrochemical measurements

Three electrodes system were utilized on photo-electrochemical measurements in various aqueous solutions with a Potentiostat/Galvanostat (HABF5001, HOKUTO DENKO) in the 50 mL quartz beaker. The flatband potentials of samples were obtained by the Mott–Schottky plots using a potentiostat (HZ3000, Hokuto Denko). Working electrodes were fabricated as follows: a mixture of TiO_2 or N-TiO_2 powders (1 g for each) with water (2 mL) was grinded to well-dispersed suspension by an agate mortar. And, the prepared suspension was spread onto the ITO-glass (10 $\Omega\,cm^{-2}$) by squige method and drying in air at room temperature. The film mass of electrodes was adjusted to be 1.20 ± 0.050 mg/cm^2 (film thickness: ca. 80–90 μm). Platinum wire and Ag/AgCl electrodes were used as auxiliary and reference electrodes, respectively. All potentials were converted from vs. Ag/AgCl into vs. NHE. The photo-irradiation was performed using a 500 W xenon lamp (Optical Modulex SX-UI501XQ, Ushio Inc.) through different low cut-off filters (Asahi Technoglass Co. Ltd.). The photo-electrochemical cell was placed at photo-intensity by 35 mW cm^{-2} at 365 nm under full arc from the xenon lamp measured by CSU-365 radiometer (Cosmo Bio Co., Ltd.). It was confirmed that the photo-intensity was strong enough to obtain saturated potentials on the film electrode. The characteristics of the low cut-off filters were as follows: λ > 510 nm for O-54, λ > 500 nm for Y-52, λ > 485 nm for Y-50, λ > 455 nm for Y-48, λ > 420 nm for Y-45, λ > 400 nm for Y-43, λ > 350 nm for L-39, λ > 340 nm for UV-37, λ > 320 nm for UV-35, λ > 300 nm for UV-33 and λ > 270 nm for UV-31. For example, the O-54 transmits the light of wavelength longer than 510 nm, and it exhibits ca. 50% light transmittance at λ = 540 nm. The measurements of photo-charging and photocurrent were performed on the N-TiO_2 and TiO_2 in the presence of acetic acid in order to understand the photocatalytic system for the decomposition of acetic acid, although an electrolyte involving such organic compounds as methanol was often used as hole scavengers. The photo-charged potentials were recorded in 0.25 M Na_2SO_4 involving 0.25 M acetic acid (pH 2.5). In order to understand electron transfer from the photo-charged N-TiO_2 into various kinds of redox species, each aqueous solution (1.0 mL) involving 1.0 mM H_2PtCl_6, $HAuCl_4$, $AgNO_3$ and $Cu(NO_3)_2$ was added into the photo-charged N-TiO_2 of three electrodes system. The pH of each solution was adjusted to ca. 2.0–2.5. Photocurrents of the TiO_2 and N-TiO_2 were recorded in 0.25 M Na_2SO_4 involving 0.25 M acetic acid (pH 2.5). The aqueous solutions were bubbled vigorously by N_2 gas for 30 min prior to measurements.

2.4. Photocatalytic reactions

The photo-induced reduction of methyl viologen (MV^{2+}) was performed on N-TiO_2 in ethanol aqueous solution in an optical quartz cell. The prepared solution consists of 3 mL of 1.0 M ethanol involving 1.0 mM MV^{2+}. The pH of solutions was adjusted to ca. 8.5 by sodium hydroxide aqueous solution. The photocatalytic reduction of H^+ into H_2 was performed in the suspension of TiO_2 or N-TiO_2 with methanol aqueous solution in a Pyrex test tube (volume: 20 mL). The prepared solution (pH 2.1) consists of 10 mL of 0.5 M methanol and 130 μL of 1.93×10^{-2} M H_2PtCl_6 aqueous solution. Prior to photochemical reactions, the suspension was bubbled and the gas-phase was purged by Ar gas at 298 K. Photoreduction of MV^{2+} into MV^+ or Pt^{4+} into Pt particles was determined by UV–vis spectroscopic technique. The amounts of evolved H_2 were analyzed by GC (Ohkura, Model-802; column: MS-5A; carrier gas: Ar) equipped with a thermal conductivity detector (TCD).

3. Results and discussion

3.1. Characterization of N-TiO_2

From the result of XRD measurement, it was observed that the N-TiO_2 prepared by calcination at 673 K has anatase structure with the crystallite size of ca. 32 nm from Scherrer equation.

In our early report [25], the XPS N 1s peak of N-TiO_2 was shown at ca. 397–401 eV, which were similar findings reported by Chen and Burda [15] and Valentin et al. [19]. The quantity of nitrogen species on N-TiO_2 was estimated to be ca. 0.34 at.% as N/Ti. According to Valentin et al. [19], the N 1s peak is possibly due to a variety of nitrogen species: substitutional (O–Ti–N) and/or interstitial (NO, NO_2 or NH_x) nitrogen species in the TiO_2 matrix. Incidentally, the N-doping states stably exist on the N-TiO_2 even after evacuation of the N-TiO_2 at 673 K, evidenced by intensive signal owing to $^{\bullet}N$ radicals under photo-irradiation in the presence of O_2 by electron spin resonance (ESR) spectroscopic measurements [31]. From these results, the nitrogen species is not simply adsorbed on the surface, but it is chemically bound and stable onto the TiO_2 matrix in any forms of substitution and interstition of nitrogen species.

UV–vis absorption spectra of TiO_2 and N-TiO_2 are shown in Fig. 1. The absorption edge (E_g) of both TiO_2 and N-TiO_2 are estimated by threshold against energy ($h\nu$). A band at ca. 3.1 eV (400 nm) is attributable to band gap transition in the spectrum of TiO_2. On the other hand, N-TiO_2 exhibits a band at ca. 3.1 eV (400 nm) together with a broad band in visible region at the center of ca. 2.8 eV (450 nm). The absorption in visible region in the spectrum of N-TiO_2 is due to the excitation of electrons from localized N-doping level in the band gap [5,20]. It should be noted that the E_g of N-TiO_2 scarcely changes by doping nitrogen species with low concentration (0.34 at.% as N/Ti) into TiO_2.

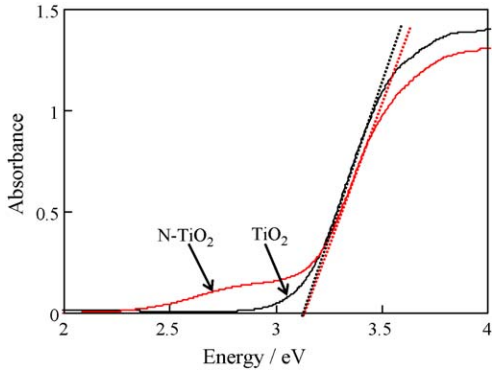

Fig. 1. UV–vis absorption spectra of TiO_2 and N-TiO_2. Dotted lines show threshold against energy ($h\nu$).

3.2. Flatband potentials of the N-TiO_2 and TiO_2

Fig. 2 shows the Mott–Schottky plots (C^{-2} vs. E) of the N-TiO_2 and TiO_2 electrodes in 0.25 M Na_2SO_4 involving 0.25 M acetic acid (pH 2.5). As shown in Fig. 2, the slope of the Mott–Schottky plots is influenced by modulation frequency (1000 and 10,000 Hz), which may be related to the donor density of the film electrodes formed by the aggregated TiO_2 nano-particles. However, the flatband potentials for both electrodes are almost the same at different modulation frequency, and they are estimated to be ca. −0.35 V vs. NHE (pH 2.5) by threshold against E, respectively. This result suggests that the flatband potential of the N-TiO_2 is not influenced by small amounts of nitrogen species doped into TiO_2.

3.3. Photocurrent measurements of the N-TiO_2 and TiO_2

Fig. 3 shows I_{ph} (photocurrent)–V (potential) curves on N-TiO_2 and TiO_2 in 0.25 M Na_2SO_4 involving 0.25 M acetic acid (pH 2.5) under photo-irradiation through different low cut-off filters: Y-52, Y-45, L-39 and UV-35. As shown in Fig. 3, the N-TiO_2 electrode exhibits anodic photocurrents under UV-light and/or visible light irradiation. On the other hand, the TiO_2 exhibits photocurrents under UV-light irradiation, while it does little under visible light irradiation. It is considered that the anodic photocurrents on both electrodes are induced by the photo-oxidation of organic compounds and/or water. The photocurrents of electrodes are observed at more anodic than the zero-current potentials, where the anodic photocurrent becomes zero. The zero-current potentials for the N-TiO_2 and TiO_2 are observed at ca. −0.25 V vs. NHE under photo-irradiation through UV-35, at ca. −0.15 V through L-39, respectively, and those only for the N-TiO_2 are at ca. +0.40 V through Y-45, at ca. +0.55 V through Y-52.

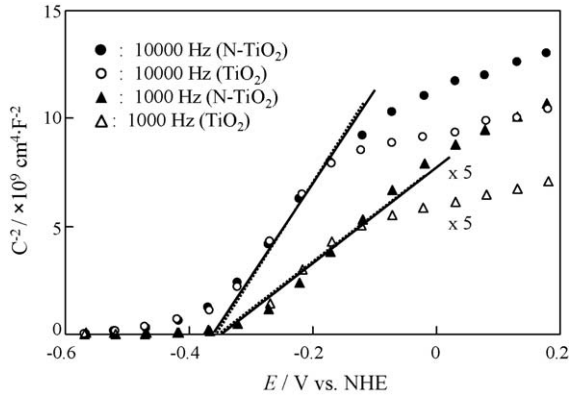

Fig. 2. Mott–Schottky plots of N-TiO_2 and TiO_2 electrodes at the modulation frequency of 1000–10,000 Hz. The measurements were performed in 0.25 M Na_2SO_4 involving 0.25 M acetic acid (pH 2.5).

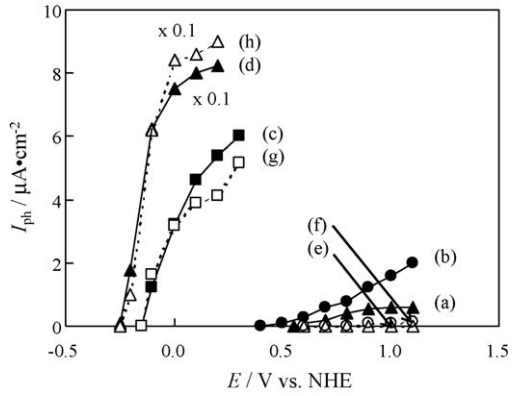

Fig. 3. I_{ph} (photocurrent)–V (potential) curves on N-TiO_2 (a–d) and TiO_2 (e–h) through different low cut-off filters: Y-52 (a, e), Y-45 (b, f), L-39 (c, g) and UV-35 (d, h). The measurements were performed in 0.25 M Na_2SO_4 involving 0.25 M acetic acid (pH 2.5).

3.4. Photo-charge and discharge properties of the N-TiO_2 and TiO_2

The effect of photo-charge on N-TiO_2 and TiO_2 electrodes was investigated in 0.25 M Na_2SO_4 involving 0.25 M acetic acid (pH 2.5). It should be noted that the photo-charged potentials stand for the Fermi levels, where the photo-induced electrons are accumulated, accompanied by oxidation of hole scavengers. Fig. 4 shows potential change of the N-TiO_2 and TiO_2 electrodes under photo-irradiation as a function of low cut-off filters. Both N-TiO_2 and TiO_2 electrodes show unchanging potentials at ca. +0.7 V vs. NHE (pH 2.5) after a while, respectively, under dark condition. As shown in Fig. 4, the TiO_2 exhibits a cathodic potential shift under UV-light irradiation, although it does little potential shift under visible light irradiation. On the other hand, visible light irradiation of the N-TiO_2 shows cathodic potential shifts, having potentials in plateau at ca. +0.35 V. Furthermore, the N-TiO_2 shows cathodic potential shift up to ca. −0.35 V under UV-light irradiation. Therefore, we assume that the visible light response is associated with the presence of N-doping states on N-TiO_2, and the plateau at ca. +0.35 V in the potential is probably correlated with the numbers of limited photo-induced electrons owing to small amounts of N-doping state, and/or with much numbers of OVs created by the charge compensation of N-doping. Also, it is confirmed that the

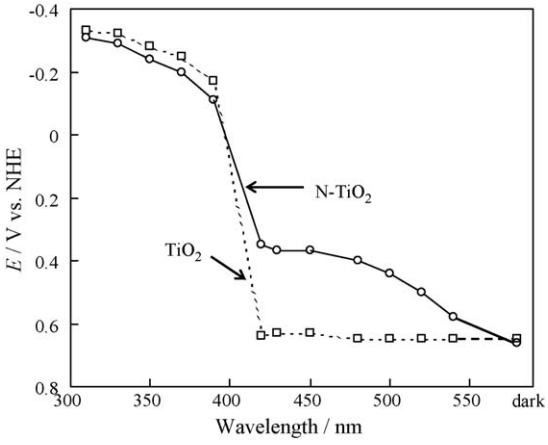

Fig. 4. Dependence of the photo-charged potentials on N-TiO_2 and TiO_2 using different low cut-off filters. The measurements were performed in 0.25 M Na_2SO_4 involving 0.25 M acetic acid (pH 2.5). Each photo-charged potential was plotted at the wavelength by ca. 50% light transmittance through low cut-off filters.

photo-charged potentials at ca. −0.33 V for N-TiO_2 and at ca. −0.35 V for TiO_2 under photo-irradiation through UV-31 correspond with the flatband potentials at ca. −0.35 V for both electrodes estimated from the Mott–Schottky plots, respectively, as shown in Fig. 2. Moreover, the photo-charged potentials in Fig. 4 roughly correspond with zero-current potentials estimated in Fig. 3: at ca. +0.55 V under photo-irradiation through Y-52, at ca. +0.40 V through Y-45, at ca. −0.15 V through L-39, and at ca. −0.25 V through UV-35, respectively.

Fig. 5 shows the processes for photo-charge under UV-light and/or visible light irradiation, and subsequent discharge at 40 nA cm^{-2} under dark condition on the TiO_2 and N-TiO_2 electrodes. From Fig. 5, following results are pointed out: (i) the photo-charged TiO_2 under photo-irradiation through UV-35 shows the potential shift up to ca. −0.27 V vs. NHE, followed by a faradic discharge curve having plateau at ca. −0.11 and ca. +0.35 V as shown in Fig. 5(a); (ii) the photo-charged N-TiO_2 through UV-35 and through L-39 shows potential shifts up to ca. −0.25 V and ca. −0.11 V, respectively, followed by subsequent discharge in Fig. 5(b and c); (iii) the photo-charged N-TiO_2 through Y-45 shows the potential shift up to ca. +0.35 V, followed by a subsequent discharge as shown in Fig. 5 (d). Therefore, the sub-band structures of N-TiO_2 are found to exhibit similar with those of TiO_2 except for the presence of N-doping states. Here, three potential regions of TiO_2 and N-TiO_2 are defined as the potential at ca. −0.35 to −0.10 V for the α potential region, that at ca. −0.10 to +0.35 V for the β and that at ca. +0.35 to +0.65 V for the γ below the conduction band of the N-TiO_2.

In order to clarify three potential regions (α, β and γ) in Fig. 5, the sub-band structures of N-TiO_2 were investigated by photoluminescence (PL) measurements. As shown in Fig. 6[I], the PL spectra at ca. 1.5–3.0 and ca. 1.5–3.5 eV are observed by excitation at 3.5 and 4.6 eV (UV-light) on the N-TiO_2, respectively. Similar phenomena are also observed on the TiO_2. The excitation and PL spectra are attributable to the electron transfer from the ground state to the conduction band, and its radiative decay from various energy sub-band levels to ground states of TiO_2 and N-TiO_2, respectively. From these results, it is found that the energy levels for sub-band structures of N-TiO_2 are similar with those of TiO_2. It should be noted that the N-TiO_2 shows little emission excited by visible light at ca. 2.7 eV although the N-TiO_2 exhibits absorption in visible region as shown in Fig. 1. The reasons for little emission from the N-TiO_2 under visible light irradiation would be explained as follows: the photo-excited electrons from N-doping states are

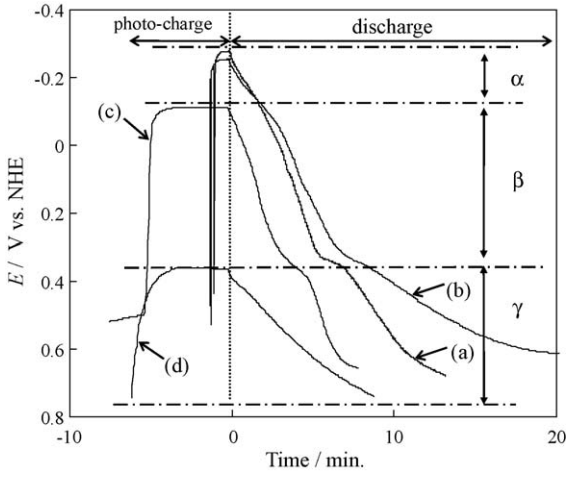

Fig. 5. Potential change on TiO_2 under photo-irradiation through UV-35 (a), and that on N-TiO_2 through UV-35 (b), through L-39 (c), through Y-45 (d); and their corresponding discharge processes. The measurements were performed in 0.25 M Na_2SO_4 involving 0.25 M acetic acid (pH 2.5).

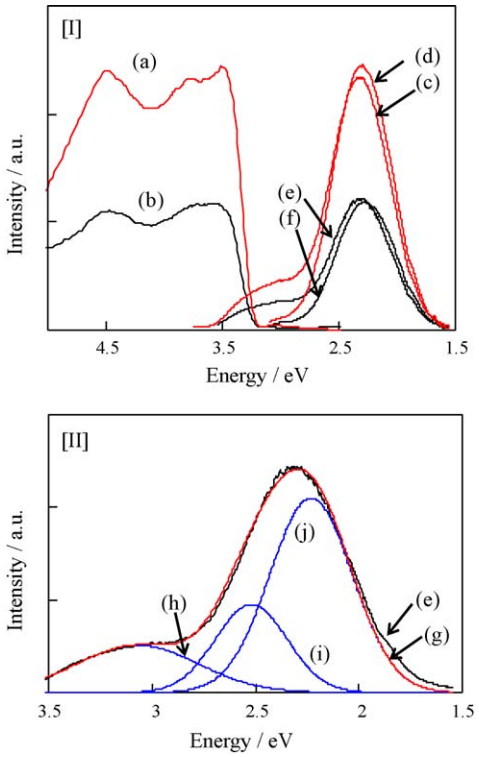

Fig. 6. Excitation (a, b) and emission (c–f) spectra for TiO_2 (a, c, and d) and N-TiO_2 (b, e, and f) [I], and fitting the original (e) into (g) composed by three Gaussian bands (h–j) [II]. The excitation and emission spectra were recorded at liquid nitrogen temperature by monitoring at 2.3 eV for (a, b), at 3.5 eV for (d, f), and at 4.6 eV for (c, e), respectively.

too small and too deeply trapped on OVs to detect emission even at liquid nitrogen temperature. Here, we assume that the N-TiO_2 (e) can be fitted by three Gaussian bands at the center of ca. 3.0 eV (h), of ca. 2.5 eV (i) and of ca. 2.2 eV (j) as shown in Fig. 6[II], since PL spectra of anatase TiO_2 are known to consist of three kinds of intrinsic states: self-trapped excitons, OVs and/or surface states [27,32]. Taking the results of potential regions (α, β and γ) in Fig. 5 into consideration, it is confirmed that the N-TiO_2 involves three types of sub-band levels at ca. −0.35 to −0.10 eV for the α potential region, at ca. −0.10 to +0.35 eV for the β, and at ca. +0.35 to +0.65 eV vs. NHE for the γ are attributable to the self-trapping excitons for the α, to the F center (OVs trapped two electrons) for the β, and to the F^+ center (OVs trapped one electron) and/or Ti^{3+} adjacent to OVs for the γ, respectively.

3.5. Potentiality for the reduction of various kinds of redox species on the N-TiO_2

So far, we have demonstrated the sub-band levels (α, β and γ potential regions) of the N-TiO_2, and the visible light irradiation of the N-TiO_2 causes an accumulation of electrons into the sub-band level of the γ potential region. In order to understand electron transfers from the photo-excited N-TiO_2 to redox species, effect of such redox species as MV^{2+}, H^+, Cu^{2+}, Ag^+, Pt^{4+}, Au^{3+} ions and O_2 molecules was investigated.

First, the photo-reduction of MV^{2+} into MV^+ in ethanol aqueous solution (pH 8.5) was performed on the N-TiO_2 through different low cut-off filters. The MV^{2+} by itself is not photo-reduced under photo-irradiation through UV-35, and the MV^+ exhibits absorption at ca. 450–800 nm when the MV^{2+} is photo-reduced. As shown in Fig. 7, it is observed that both N-TiO_2 and TiO_2 exhibit photo-reduction of MV^{2+} into MV^+ only under UV-light irradiation. Taking at −0.45 V for E^0 (MV^+/MV^{2+}), it is confirmed that photo-excited

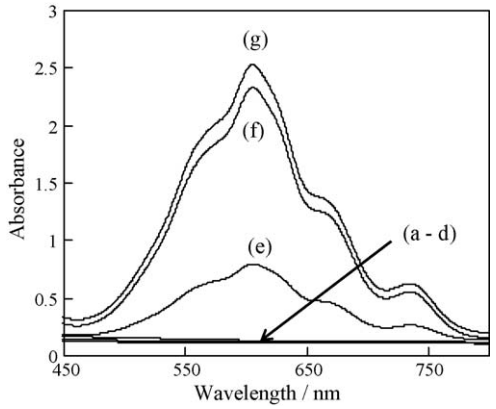

Fig. 7. Absorption spectra of methyl viologen aqueous solutions in the presence of N-TiO_2 through different low cut-off filters: under un-irradiation (a), Y-52 (b), Y-45 (c), Y-43 (d), L-39 (e), UV-37 (f) and UV-35 (g).

N-TiO_2 under visible light irradiation does not have potentiality for the reduction of MV^{2+} into MV^{+}.

Second, photo-reduction of Pt^{4+} ions and simultaneous H_2 evolution were investigated in methanol aqueous solution on the N-TiO_2 and TiO_2 under photo-irradiation through different low cut-off filters. The Pt ions by itself are not photo-reduced under photo-irradiation through UV-35. And the Pt particles exhibit broad absorption in visible region when the Pt ions are photo-reduced. An increase of absorption at ca. 400–800 nm owing to Pt particles is observed on the N-TiO_2 not only under visible light but also under UV-light irradiation as shown in Fig. 8[I], while that is observed on the TiO_2 only under UV-light irradiation. Each absorbance for the N-TiO_2 and TiO_2 is plotted as shown in Fig. 8[II] (h and i). Incidentally, the photo-reduction of H^+ to form H_2 is observed on the N-TiO_2 and TiO_2 only under UV-light irradiation as shown in Fig. 8[II] (j and k). Taking the photo-charged potential shifts of the N-TiO_2 and TiO_2 in Fig. 4 and the redox potentials at +0.742 V for E^0 ($[PtCl_6]^{4-}/Pt + 6Cl^-$), at 0 vs. NHE (pH 0) for E^0 ($2H^+/H_2$) [33,34] into consideration, we assume that the photo-induced electron transfer takes place from the sub-band level of the γ potential region into Pt^{4+} ions to form Pt particles, while from that of the α into H^+ to form H_2, respectively.

Third, effect of redox species such as Cu^{2+}, Pt^{4+}, Ag^+, Au^{3+} ions and O_2 molecules on the photo-charged N-TiO_2 was investigated by monitoring potential shifts. Fig. 9 shows cathodic potential shifts up to ca. +0.35 V on N-TiO_2 under photo-irradiation through Y-45, and subsequent discharge of the photo-charged N-TiO_2 by adding redox species. It is found that the anodic potential shift depends on the kinds of redox species: at ca. +0.43 V for no addition (self-discharging), at ca. +0.43 V by Cu^{2+}, at ca. +0.63 V by Ag^+, at ca. +0.65 V by O_2 molecules, at ca. +0.72 V by Pt^{4+} and at ca. +1.09 V by Au^{3+} ions, respectively. These results indicate that the photo-excited N-TiO_2 under visible light irradiation accumulates electrons on the sub-band level of the γ, and they transfer into such redox species as Pt^{4+}, Ag^+, Au^{3+} ions and O_2 molecules except for Cu^{2+} ions. Thus, this technique is unique and successful to understand electron transfer from the photo-charged N-TiO_2 to the redox species.

3.6. The energy diagram of the N-TiO_2

The energy levels for sub-band structures of N-TiO_2 have been proposed from the photo-electrochemical and spectroscopic measurements as shown in Fig. 10. The theoretical calculations by Valentin et al. [19] showed that the N_{2p} states of the substitutional (N_s) or interstitial (N_i) species in N-doped TiO_2 are located at 0.59 eV for diamagnetic N_s^-, at 0.14 eV for radical

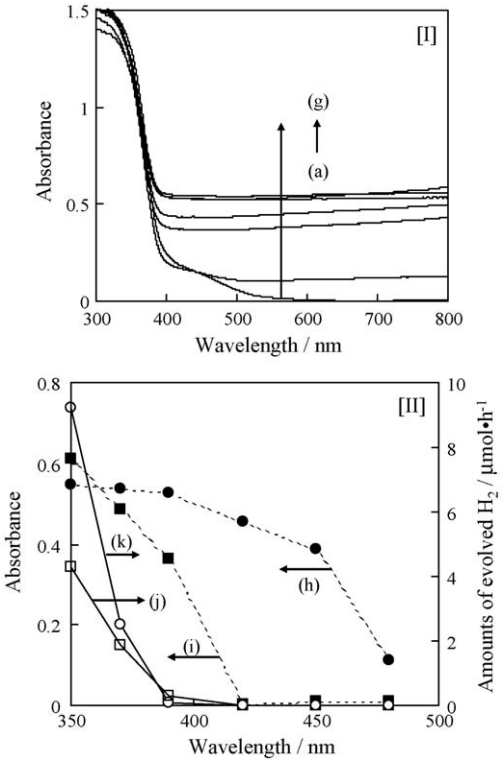

Fig. 8. [I] Absorption spectra of platinum species deposited on N-TiO_2 in methanol aqueous solution through different low cut-off filters: under un-irradiation (a), Y-48 (b), Y-45 (c), Y-43 (d), L-39 (e), UV-37 (f) and UV-35 (g). [II] Change of absorbance at 600 nm (h, i) and amounts of evolved H_2 (j, k) on N-TiO_2 (h, j) and TiO_2 (i, k) as a function of low cut-off filters. Each absorbance and amounts of evolved H_2 was plotted at the wavelength by ca. 50% light transmittance through low cut-off filters.

$^{\bullet}N_s$; at 0.75 eV for N_i^- and at 0.73 eV for $^{\bullet}N_i$, respectively, above the valence band edge. Taking the absorption in the visible light region from 2.3 to 3.0 eV of the N-TiO_2 involving different kinds of nitrogen species into consideration, it is assumed that the heterogeneous N-doping states are photo-excited to the conduction band. When the N-doping level of N-TiO_2 is photo-excited under visible light irradiation, the photo-induced holes can oxidize

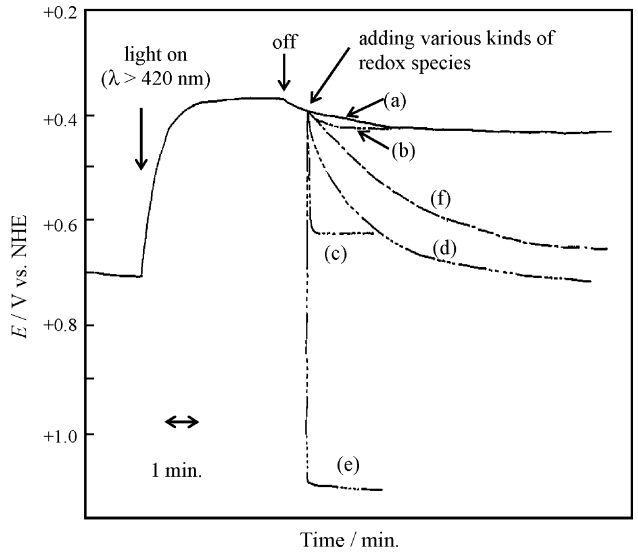

Fig. 9. Potential change of the N-TiO_2 electrode for photo-charge under photo-irradiation through Y-45 in 0.25 M Na_2SO_4 involving 0.25 M acetic acid (pH 2.5) and for discharge after no addition (a), after adding aqueous solutions involving Cu^{2+} (b), Ag^+ (c), Pt^{4+} (d), Au^{3+} ions (e) and O_2 molecules (f) into the photo-charged N-TiO_2.

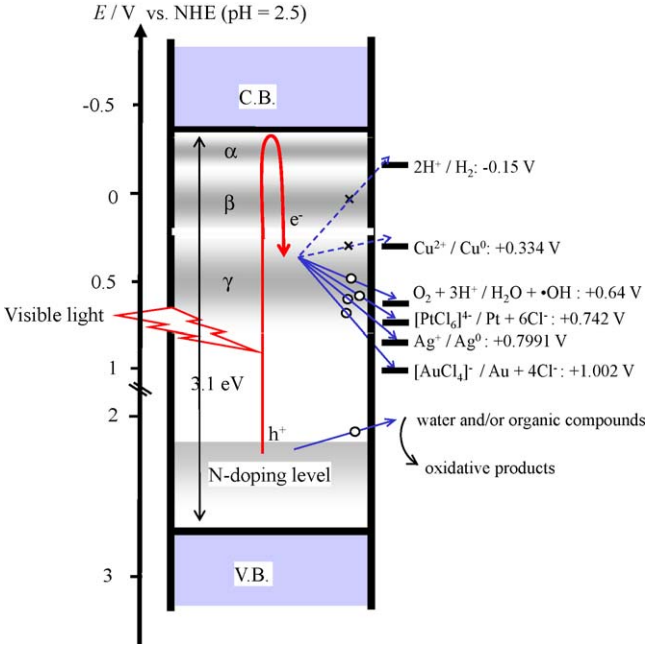

Fig. 10. Energy diagram of N-TiO_2 and photo-induced charge transfer into various kinds of redox species under visible light irradiation. The V.B. and C.B. stand for valence band and conduction band, respectively. The energy levels of sub-bands at the α, β, γ potential regions, N-doping levels on the N-TiO_2; and potentials of various kinds of redox species are shown in vs. NHE (pH 2.5). Signs of circle and cross stand for energetically favorable and unfavorable electron transfers, respectively.

water [12] and/or organic compounds, while photo-induced electrons are accumulated at the sub-band of the γ by way of conduction band. Subsequently, when various kinds of redox species are added into the photo-charged N-TiO_2, the accumulated electrons at the γ potential region are not able to reduce MV^{2+}, H^+, Cu^{2+} ions, but able to do O_2 molecules, Pt^{4+}, Ag^+ and Au^{3+} ions. It should be noted that redox potentials of various kinds of species are shown as follows: at 0 V for E^0 ($2H^+/H_2$), at +0.334 V for E^0 (Cu^{2+}/Cu^0), at +0.742 V for E^0 ($[PtCl_6]^{4-}/Pt + 6Cl^-$), at +0.79 V for E^0 ($O_2 + 3H^+/H_2O + {}^\bullet OH$), at +0.7991 V for E^0 (Ag^+/Ag^0) and at +1.002 V for E^0 ($[AuCl_4]^-/Au + 4Cl^-$) vs. NHE (pH 0) [33–35]. Fig. 10 involves potentials at vs. NHE (pH 2.5) for the redox species as mentioned above. Taking these redox potentials into consideration, it was demonstrated that the photo-excited N-TiO_2 under visible irradiation works for reduction of redox species not directly through the conduction band, but through the sub-band of the γ. In particular, the electron transfer from the photo-excited N-TiO_2 into O_2 molecules may lead to form such active oxygen species as •OH radicals, followed by oxidation of organic substrates. These findings shed light on a mechanism for the photocatalytic decomposition of environmental pollutants on the N-TiO_2 under visible light irradiation.

4. Conclusions

Photo-electrochemical and optical properties of N-TiO_2 were investigated. Following conclusions shed light on a mechanism for the photocatalytic reaction under visible light irradiation. The results obtained in this study suggest as follows:

(1) The energy levels for sub-band structures of N-TiO_2 consist of three types of intrinsic states: α, β and γ potential regions below the conduction band and the N-doping levels above the valence band.
(2) The photo-excitation of N-TiO_2 causes the accumulation of electrons into the sub-band level of the γ potential region under visible light irradiation.
(3) Subsequently, the electron transfer takes place from the photo-charged N-TiO_2 into such redox species as O_2 molecules, Pt^{4+}, Ag^+ and Au^{3+} ions having more anodic potential than the γ.

Acknowledgements

The authors wish to acknowledge useful discussion and support given by Professors Masakazu Anpo and Masaya Matsuoka (Osaka Prefecture University).

References

[1] A. Fujishima, T.N. Rao, D.A. Tryk, J. Photochem. Photobiol. C: Photochem. Rev. 1 (2000) 1–21.
[2] M. Graetzel, J. Photochem. Photobiol. C: Photochem. Rev. 4 (2003) 145–153.
[3] D. Chatterjeeand, S. Dasgupta, J. Photochem. Photobiol. C: Photochem. Rev. 6 (2005) 186–205.
[4] K. Maeda, K. Teramura, D. Lu, T. Takata, N. Saito, Y. Inoue, K. Domen, Nature 440 (2006) 295.
[5] R. Asahi, T. Morikawa, K. Aoki, Y. Taga, Science 293 (2001) 269–271.
[6] S. Sato, Chem. Phys. Lett. 123 (1986) 126–128.
[7] C. Burda, Y. Lou, X. Chen, A.C.S. Samia, J. Stout, J.L. Gole, Nano Lett. 3 (2003) 1049–1051.
[8] S. Sato, R. Nakamura, S. Abe, Appl. Catal. A: Gen. 284 (2005) 131–137.
[9] H. Irie, Y. Watanabe, K. Hashimoto, J. Phys. Chem. B 108 (2003) 5483–5486.
[10] Y. Sakatani, J. Nunoshige, H. Ando, K. Okusako, H. Koike, T. Takata, J.N. Kondo, M. Hara, K. Domen, Chem. Lett. 32 (2003) 1156–1157.
[11] O. Diwald, T.L. Thompson, E.G. Goralski, S.D. Walck, J.T. Yates Jr., J. Phys. Chem. B 108 (2004) 52–57.
[12] R. Nakamura, T. Tanaka, Y. Nakato, J. Phys. Chem. B 108 (2004) 10617–10620.
[13] S. Sakthivel, M. Janczarek, H. Kisch, J. Phys. Chem. B 108 (2004) 19384–19387.
[14] G.R. Torres, T. Lindgren, J. Lu, C.-G. Granqvist, S.-E. Lindquist, J. Phys. Chem. B 108 (2004) 5995–6003.
[15] X. Chen, C. Burda, J. Phys. Chem. B 108 (2004) 15446–15449.
[16] J.L. Gole, J.D. Stout, C. Burda, Y. Lou, X. Chen, J. Phys. Chem. B 108 (2004) 1230–1240.
[17] M. Bazil, E.H. Morales, U. Diebold, Phys. Rev. Lett. 96 (2006), 026103/1–026103/4.
[18] S. Livraghi, A. Votta, M.C. Paganini, E. Giamello, Chem. Commun. 4 (2005) 498–500.
[19] C.D. Valentin, G. Pacchioni, A. Selloni, S.S. Livraghi, E. Giamello, J. Phys. Chem. B 109 (2005) 11414–11419.
[20] S. Livraghi, M.C. Paganini, E. Giamello, A. Selloni, C.D. Valentin, G. Pacchioni, J. Am. Chem. Soc. 128 (2006) 15666–15671 (and references therein).
[21] S. In, A. Orlov, F. Garcia, M. Tikhov, D.S. Wright, R.M. Labbert, Chem. Commun. 40 (2006) 4236–4238.
[22] Y. Nakano, T. Morikawa, T. Ohwaki, Y. Taga, Appl. Phys. Lett. 86 (2005), 132104/1-132104/3.
[23] K. Hashimoto, H. Irie, A. Fujishima, Jpn. J. Appl. Phys. 44 (2005) 8269–8285.
[24] S. Higashimoto, K. Takamatsu, M. Azuma, M. Kitano, M. Matsuoka, M. Anpo, Catal. Lett. 122 (2008) 33–36.
[25] S. Higashimoto, Y. Ushiroda, M. Azuma, H. Ohue, Catal. Today 132 (2008) 165–169.
[26] S. Higashimoto, W. Tanihata, Y. Nakagawa, M. Azuma, H. Ohue, Y. Sakata, Appl. Catal. A: Gen. 340 (2008) 98–104.
[27] D. Li, H. Haneda, S. Hishita, N. Ohashi, Chem. Mater. 17 (2005) 2596–2602.
[28] A.V. Emeline, N.V. Sheremetyeva, N.V. Khomchenko, V.K. Ryabchuk, N. Serpone, J. Phys. Chem. C 111 (2007) 11456–11462.
[29] Y. Cong, J. Zhang, F. Chen, M. Anpo, J. Phys. Chem. C 111 (2007) 6976–6982.
[30] M. Kitano, K. Funatsu, M. Matsuoka, M. Ueshima, M. Anpo, J. Phys. Chem. B 110 (2006) 25266–25272.
[31] S. Higashimoto, Y. Ushiroda, M. Azuma, J. Nanosci. Nanotechnol. (2009) in press.
[32] Y. Lei, L.D. Zhang, G.H. Li, X.Y. Zhang, C.H. Liang, W. Chen, S.X. Wang, Appl. Phys. Lett. 78 (2001) 1125–1127.
[33] D.T. Sawyer, A. Sobkowiak, J.L. Roberts, Electrochemistry for Chemists, 2nd ed., John Wiley & Sons, Inc., New York, 1996.
[34] Electrochem. Soc. Japan, Denki Kagaku Binran, 5th ed., Maruzen, Tokyo, 2000, p. 91 (in Japanese).
[35] M. Pourbaix, Atlas of Electrochemical Equilibria in Aqueous Solutions, Pergamon Press Ltd., London, 1966.